New Journal of Physics

The open access journal at the forefront of physics

CrossMark

PAPER

Efficient simulation of non-Markovian system-environment interaction

Robert Rosenbach[1], Javier Cerrillo[2,3,4], Susana F Huelga[1], Jianshu Cao[2] and Martin B Plenio[1,4]

[1] Institute of Theoretical Physics, Universität Ulm, Albert-Einstein-Allee 11, D-89069 Ulm, Germany
[2] Massachusetts Institute of Technology, 77 Massachusetts Avenue, Cambridge, Massachusetts 02139, USA
[3] Institute of Theoretical Physics, Technische Universität Berlin, Hardenbergstr. 36, D-10623 Berlin, Germany
[4] Authors to whom any correspondence should be addressed.

E-mail: cerrillo@tu-berlin.de and martin.plenio@uni-ulm.de

Abstract

In this work, we combine an established method for open quantum systems—the time evolving density matrix using orthogonal polynomials algorithm—with the transfer tensors formalism, a new tool for the analysis, compression and propagation of non-Markovian processes. A compact propagator is generated out of sample trajectories covering the correlation time of the bath. This enables the investigation of previously inaccessible long-time dynamics with linear effort, such as those ensuing from low temperature regimes with arbitrary, possibly highly structured, spectral densities. We briefly introduce both methods, followed by a benchmark to prove viability and combination synergies. Subsequently we illustrate the capabilities of this approach at the hand of specific examples and conclude our analysis by highlighting possible further applications of our method.

1. Introduction

Ranging from condensed matter physics or quantum technologies to biological chemistry, the experimental ability to accurately probe and analyze quantum systems in strong contact with highly structured environmental degrees of freedom for extended periods of time has become a reality [1–6]. Under certain conditions it is possible to model the observations by using approximate methods such as perturbative approaches [7, 8], frequently supplemented with Markovian assumptions [9–11]. Beyond their regime of validity, the task of exactly treating the dynamics of open quantum systems faces the challenge of an unfavorable scaling in the required resources. Nevertheless, many tools have been developed that address a wide variety non-Markovian scenarios for short time simulations or for specific conditions and approximations.

Exact procedures such as projection operator techniques serve to derive formally exact master equations that can involve a memory kernel as in the Nakajima–Zwanzig formalism [12] or have a generator that is local in time, like the so-called time-convolutionless master equations [13]. The path integral formulation [14] provides an alternative perspective especially suitable for harmonic baths thanks to the Feynmann–Vernon influence functional [15]. Practical implementation of these formal treatments requires perturbative expansions in terms of some specific parameter, be it weak damping, high temperature, short memory time, or short simulation time [16–19]. An exhaustive list is not within the scope of this work, but some additional instances include the non-Markovian quantum state diffusion approach [20], the hierarchy of equations of motion (HEOM) [17, 21], iterative path integral resummations [22], multilayer multiconfigurational time-dependent Hartree methods [23], explicit computation of the Nakajima–Zwanzig memory kernel [24, 25] and the time-convolutionless kernel [26] or mixed quantum–classical methods [27–29]. Alternatively, the harmonic bath assumption renders possible the use of stochastic Gaussian sampling of the bath operator or the influence functional [30–33]. Hybrid stochastic-deterministic methods have appeared recently as well [34]. Another option is to simulate the density

matrix of both the system and the complete environment by employing an efficient description of the bath or gradually introducing select degrees of freedom [35–37]. To this class of methods belongs the 'time evolving density matrix using orthogonal polynomials algorithm' (TEDOPA) [38, 39]. This method uses a stable numerical transformation to map the environment into a chain of harmonic oscillators, which can then be simulated together with the system using efficient quantum many body techniques [40]. Although a more thorough discussion follows below, as compared to other simulation methods TEDOPA is especially suitable for simulation of quadratic harmonic baths with arbitrarily shaped spectral-densities in the low-temperature regime and is not restricted to small coupling or Ohmic baths.

For any exact simulation method it is generally the case that the size of the propagator or that of the stochastic sample scales unfavorably with the time length of the simulation or the corresponding perturbative expansion order. Then the question arises whether there are regimes where this scaling can be mitigated in some form, i.e. if an effective propagator of a reduced size can be extracted with the intention of facilitating long-time simulations. In the present work we address this question combining TEDOPA with a tool quantifying the bath's back-action on the system as in the Nakajima–Zwanzig formalism. This tool is known as the transfer tensor method (TTM) [41], which has been shown to provide considerable acceleration in the context of non-Markovian open quantum system simulations as well as in large classical systems [42]. This is achieved by blackbox learning from sample exact trajectories for some short initial period and subsequent generation of a compact multiplicative propagator for the system degrees of freedom alone. This propagator is the set of discrete elements of the integration of the Nakajima–Zwanzig equation which, similarly to the memory kernel, decay at the rate of the bath correlation function. This justifies the definition of a memory cutoff, corresponding to the maximum time for which non-Markovian effects are to be considered. The method does not require input of a microscopic description of the problem and just involves straightforward analysis of the evolution of the system density matrix. In this sense, TTM is directly applicable to any state propagation simulator. For a learning period longer than the environment correlation time, the propagator accurately reproduces the long time system dynamics with linear effort. Another possibility to exploit the decay of the memory effects in dissipative systems is to explicitly calculate the Nakajima–Zwanzig memory kernel [24, 25]. Although this is in general a demanding task, it is possible for specific systems and has been implemented with the help of quantum Monte-Carlo methods [25, 43] or multilayer multiconfigurational time-dependent Hartree methods [44, 45]. With TTM an explicit computation of the memory kernel is avoided and a discretized propagator is directly obtained. This propagator grows linearly with the correlation time of the bath, improving on the size of some deterministic simulation methods of linear propagation effort [17, 18]. It is a general and flexible approach that does not depend on the form of the environment or the interaction, while TEDOPA is not restricted to weak system-bath coupling, high temperatures or specific spectral densities. Therefore, they constitute ideal partners and a study of their combined performance represents a natural research question.

We start the discussion in section 2 by providing a general analysis of both TEDOPA and TTM, thereby specifying the regime in which their combination is expected to be most productive. In addition, tools for the error assessment are provided. In section 3 we provide a benchmark between the proposed combination and the exact result and confirm perfect agreement. Finally, in section 4 relevant applications of the TEDOPA-TTM combination are proposed which include Ohmic and non-Ohmic spectral densities, low temperature simulations and computations of absorption spectra.

2. The method

2.1. A numerically exact open quantum system simulator

TEDOPA [38, 39] is a numerically exact and certifiable simulation method for open quantum system dynamics [46]. It applies to general systems under linear interaction with an environment modeled by a set of independent harmonic oscillators such that the total Hamiltonian H can be split into the system, the environment and the interaction between the two as

$$H = H_{\text{sys}} + H_{\text{env}} + H_{\text{int}}, \tag{1}$$

$$H_{\text{env}} = \int_0^{x_{\text{max}}} \mathrm{d}x \, g(x) a_x^\dagger a_x, \tag{2}$$

$$H_{\text{int}} = \int_0^{x_{\text{max}}} \mathrm{d}x \, h(x)(a_x^\dagger + a_x) A. \tag{3}$$

Here $a_x^\dagger$ and a_x denote the bosonic creation and annihilation operators corresponding to the environmental mode x. The coefficients $g(x)$ can be identified as the environmental dispersion relation. The interaction term H_{int} assigns each mode a coupling strength $h(x)$ between its displacement $a_x^\dagger + a_x$ and a general system operator A.

Together with the temperature, the functions $g(x)$ and $h(x)$ characterize the harmonic environment uniquely and define the *spectral density* $J(\omega)$ as

$$J(\omega) = \pi h^2 [g^{-1}(\omega)] \frac{\mathrm{d}g^{-1}(\omega)}{\mathrm{d}\omega}. \tag{4}$$

Here $g^{-1}[g(x)] = g[g^{-1}(x)] = x$ and $g(x)$ is monotonically growing. The quantity $\frac{\mathrm{d}g^{-1}(\omega)}{\mathrm{d}\omega}\delta\omega$ can be interpreted as the number of quantized modes with frequencies between ω and $\omega + \delta\omega$ (for $\delta\omega \to 0$). We consider spectral densities subject to a hard cut-off at frequency ω_{hc}; this in turn defines the cut-off $x_{\max}$ in equations (2) and (3) as $x_{\max} = g^{-1}(\omega_{\mathrm{hc}})$.

TEDOPA uses a two-stage sequence to enable full treatment of the system and environment degrees of freedom. In a first step, an analytic transformation based on orthogonal polynomials converts the star-shaped system-environment structure into a one-dimensional geometry, where the system couples only to the first site of a semi-infinite chain of harmonic oscillators that contains only nearest-neighbour interactions. This is accomplished by use of a unitary transformation U, which defines new harmonic oscillators with creation and annihilation operators $b_n^\dagger, b_n$ given by

$$U_n(x) = h(x)p_n(x), \tag{5}$$

$$b_n^\dagger = \int_0^{x_{\max}} \mathrm{d}x \ U_n(x) a_x^\dagger. \tag{6}$$

Here $p_n(x)$ are orthogonal polynomials defined with respect to the measure $\mathrm{d}\mu(x) = h^2(x)\mathrm{d}x$ and the three-term recurrence relation

$$p_{k+1}(x) = (x - \alpha_k)p_k(x) - \beta_k p_{k-1}(x), \tag{7}$$

with $p_{-1}(x) \equiv 0$ and k a positive integer or zero. This transformation can be performed analytically for specific spectral densities [39, 47]. For arbitrarily shaped spectral densities a numerically stable approach has been developed [38, 48]. Mappings using orthogonal polynomials have been shown to be exact for quadratic Hamiltonians [49].

The recurrence relation (7) results in the one-dimensional configuration with the Hamiltonian

$$\tilde{H} = H_{\mathrm{sys}} + \eta_0 A(b_0 + b_0^\dagger) + \sum_{n=0}^\infty \omega_n b_n^\dagger b_n$$
$$+ \sum_{n=0}^\infty \eta_n (b_n^\dagger b_{n+1} + b_n b_{n+1}^\dagger). \tag{8}$$

For a linear dispersion relation $g(x) = g'x$, $\omega_n = g'\alpha_n$ and $\eta_n = g'\sqrt{\beta_{n+1}}$. Due to the form of the emerging linear geometry, this first stage of TEDOPA is coined 'chain mapping'. One dimensional quantum many body systems can be efficiently simulated with the well established time dependent density matrix renormalization group (t-DMRG) algorithm [50–52]. Its application to evaluate the dynamics of the system *and* the transformed environment constitutes the second stage of TEDOPA. The long ranged correlations appearing in the original star-shaped geometry advise against the application of t-DMRG in that picture: it is the nearest neighbor structure that makes the numerical t-DMRG approach particularly efficient. Recent works consider the possibility to use generalized matrix product state formulations for treatment of star-shaped baths as well [53].

For a complete account of TEDOPA's inner workings refer to [38, 39, 54]. Suffice it to say that three main aspects distinguish it from other open quantum-system methods. First, it does not restrict the ratio λ between inner-system couplings and system-environment couplings, unlike numerous other methods (which assume either $\lambda \gg 1$ or $\lambda \ll 1$). Second, the spectral density characterizing the system-environment interaction may assume any arbitrary shape, including a wide variety of sharp features that may be related to long-lived vibrational modes [38, 55, 56]. Such spectral densities are often encountered in spectral densities reconstructed from experimental data, e.g. in biological settings [57]. And third, while applicable to all temperatures, due to its scaling properties TEDOPA is inherently well-suited for simulations in the low-temperature domain.

Naturally, however, exact numerical methods tend to be costly and an effort to save on the associated computational demands is desirable. Where the transfer tensor method can be applied, these costs can be reduced and challenging long time simulations become accessible.

2.2. Non-Markovian dynamical maps: transfer tensor method
The transfer tensor method [41] reduces the numerical effort of TEDOPA simulations for a large class of non-Markovian environments. Its key idea is to relate the initial stages of the system's evolution to later times by efficiently determining the dynamical correlations built up between system and environment. This is achieved by the reconstruction of dynamical maps for short initial evolution times and their subsequent transformation into so-called *transfer tensors*.

A dynamical map is defined for an initial condition where the state of the system and the state of the environment are separable, and it fully determines the reduced state of the system $\rho(t)$ when applied to an initial condition $\rho(0)$

$$\rho(t) = \mathcal{E}(t, 0)\rho(0). \tag{9}$$

For a time independent Hamiltonian H such as equation (1), equation (9) is related to the solution of the time-translationally invariant Nakajima–Zwanzig equation

$$\dot{\rho}(t) = -\mathrm{i}\mathcal{L}_s\rho + \int_0^t \mathrm{d}t'\mathcal{K}(t - t')\rho(t'), \tag{10}$$

where $\mathcal{L}_s\rho = [H_{\mathrm{sys}}, \rho]$ is the Liouvillian of the system alone and $\mathcal{K}(t - t')$, is the memory kernel arising from the system-bath interaction H_{int}.

The input for TTM is a set of dynamical maps $\mathcal{E}_k = \mathcal{E}(t_k, 0)$, where a discretisation time step δt ($t_k \equiv k\delta t$) is used. These dynamical maps are obtained easily from the evolution of all distinct initial basis states of the system's density matrix. The transfer tensors are then iteratively defined by

$$T_n = \mathcal{E}_n - \sum_{m=1}^{n-1} T_{n-m}\mathcal{E}_m. \tag{11}$$

According to this definition, the transfer tensor T_k then quantifies the correlation in the dynamical map $\mathcal{E}_k$ with the non-Markovian effects built up during the previous k time steps.

Further, the discretization of the memory kernel $\mathcal{K}$ is directly related to these tensors by the time step δt

$$T_k = \mathcal{K}_k\delta t^2, \tag{12}$$

where $\mathcal{K}_k = \mathcal{K}(t_k)$ is the discretized memory kernel at time t_k. The system Hamiltonian is itself accessible from the first transfer tensor by

$$T_1 = (\mathbb{1} - \mathrm{i}\mathcal{L}_s\delta t). \tag{13}$$

These tensors can be used to propagate the system to arbitrary later times as long as they cover the relevant part of the memory kernel. Assuming a finite coherence time of the bath t_{bath}, the transfer tensors will decay sufficiently fast that a cutoff K can be defined such that $T_k = 0$ for $k > K$. Then, $\rho(t_n)$ for $n > K$ can be expressed simply as

$$\rho(t_n) = \sum_{k=1}^{K} T_k\rho(t_{n-k}). \tag{14}$$

TTM is applicable in a variety of interesting cases, scaling favorably in system size and length of the environment's correlation time. Due to its nature it also does not rely on assumptions about the system's parameters or environmental couplings. Thus it is usable as a powerful black box tool which, given initial trajectories, subsequently delivers the evolution trajectories for later times. For a more complete account of this tool refer to [41].

2.3. Synergies

The combination of both methods facilitates the simulation of open quantum systems in regimes that were previously inaccessible. Exceptionally relevant is the ability to perform long-time simulations of low-temperature, highly structured harmonic environments at merely a fraction of the computational cost which would be necessary if only TEDOPA were applied. Evidence for this is provided by simple examination of some of the features of each of the methods. On the one hand, TEDOPA is based on a matrix product operator (MPO) description of the complete system plus environment density matrix. Settings leading to low occupation numbers of environmental oscillators—such as low temperatures—are especially suitable as they reduce the MPO's number and size. In addition TEDOPA is not limited to a specific analytical form of spectral density. On the other hand, recurrence effects originating at the chain's boundary limit the time for which accurate simulation is possible. Because TTM only requires sample system trajectories for as long as bath correlations are present, the required chain length is then not anymore determined by the target simulation time. The combination of TTM and TEDOPA is therefore most useful in highly non-Markovian regimes where bath correlation times are comparable to the maximum simulation time that TEDOPA can reach before recurrences appear.

2.4. Parameters and accuracy

Here we analyze relevant parametric cutoffs for the control of the accuracy of numerical simulations that combine TEDOPA and TTM.

In the case of TEDOPA one can distinguish between parameters related to the chain mapping and to the t-DMRG propagation. The semi-infinite chain of oscillators generated by the mapping necessarily requires the truncation of both the chain length N and the Hilbert space dimension d for each oscillator at a reasonable value. Those are native TEDOPA error sources and they have a direct effect on the recurrence time of the simulation and the maximum temperature that may be simulated, respectively. It should be noted that the error incurred by these two approximations can be upper-bounded rigorously by analytical expressions [46]. The effect of other relevant parameters, namely the MPO's matrix size ($\chi \times \chi$) and the time step δt, are already well-known from the time-evolving block decimation (TEBD) algorithm [51]. To reach the accuracy required by TTM, care needs to be taken in adjusting these parameters to bound the total error of TEDOPA sufficiently. Some indications on how to accomplish this are provided in the present section.

The maximum time $t_{\max}$ before unphysical back-actions of the environment due to reflections at the end of the chain appear is related to the chain length N. Usually all chain coefficients are of the same order of magnitude and hence the simulation time $t_{\max}$ scales roughly linearly with N. This reveals one of the benefits of the application of TTM on TEDOPA: the chain length can be truncated according to the length of the bath correlation time, allocating the simulation resources properly and shortening simulation times considerably in many cases of relevance (see figure 7). The exact relationship between N and $t_{\max}$ may be derived analytically through the use of Lieb–Robinson bounds [46] or numerically by trial-and-error: by setting the chain in an initial state $|10\ldots0\rangle$ and following the evolution of the number operator n on the first site, $O = n \otimes \mathbb{1} \otimes \ldots \otimes \mathbb{1}$, until a recurrence occurs.

The second native TEDOPA parameter is the local dimension d of the single oscillators constituting the environment. For a given temperature, the occupation of the single oscillators can be determined exactly, giving a rough scale of the necessary truncation level. Some error will be introduced necessarily but this can be upper-bounded analytically as explained in [46]. On the other hand, numerical benchmark calculations with increasing local dimensions will generally yield sufficiently accurate results.

A further subtlety in the chain mapping consists in the determination of an adequate hard cutoff frequency ω_{hc} of the spectral density. For instance, the slow approach to zero for large frequencies of the Drude–Lorentz bath imposes a careful convergence check of the resulting physical behavior. For further discussions of these effects refer to [54].

While some error sources (like the cutoff in the chain length) introduce, if treated correctly, virtually no error at all, the matrix size χ necessarily does so due to the nature of the MPO. However, as already studied in the context of the TEBD algorithm, this error can be monitored during the time evolution [50]. This results in a quantity very similar to the *discarded weight* known from DMRG

$$w_{\text{discarded}} = 1 - \sum_i e_i^2. \tag{15}$$

This quantifies the deviation from the targeted state using the discarded eigenvalues e_i. This error propagates in a non-trivial fashion and it is advisable to perform convergence checks in the dynamics under variation of the size of χ. An additional source of error is derivated from the Suzuki–Trotter decomposition used in the TEBD part of TEDOPA.

It should be noted that the magnitude of the singular values kept during MPO-procedures should not fall below some threshold e_0. The transfer tensors determined by TTM do decay rapidly, falling to comparatively low magnitudes, and singular values corrupted by numerical noise deteriorates the interpretation of results as well as the propagation procedure.

Finally, for TTM the important quantity to keep track of in simulations is the norm of the memory kernel. This corresponds to the norm of the transfer tensors divided by the squared time step δt. This magnitude should exhibit a sufficiently fast decay so that the remaining tail can be neglected. Additionally, the time step δt must be such that it provides a good resolution of the features of the memory kernel.

3. Benchmark

In this section we verify the combination of TEDOPA with TTM by comparing the obtained transfer tensors with those originating from another numerically exact simulation method for non-Markovian systems under the same conditions. The chosen benchmark regime is the Ohmic Drude–Lorentz bath and the additional simulation method is the hierarchy of equations of motion (HEOM) [17].

We consider the spin-boson model (SBM) and define the (monomeric) system Hamiltonian

$$H_{\text{sys}} = \frac{1}{2}\epsilon\sigma_z + \frac{1}{2}\Delta\sigma_x. \tag{16}$$
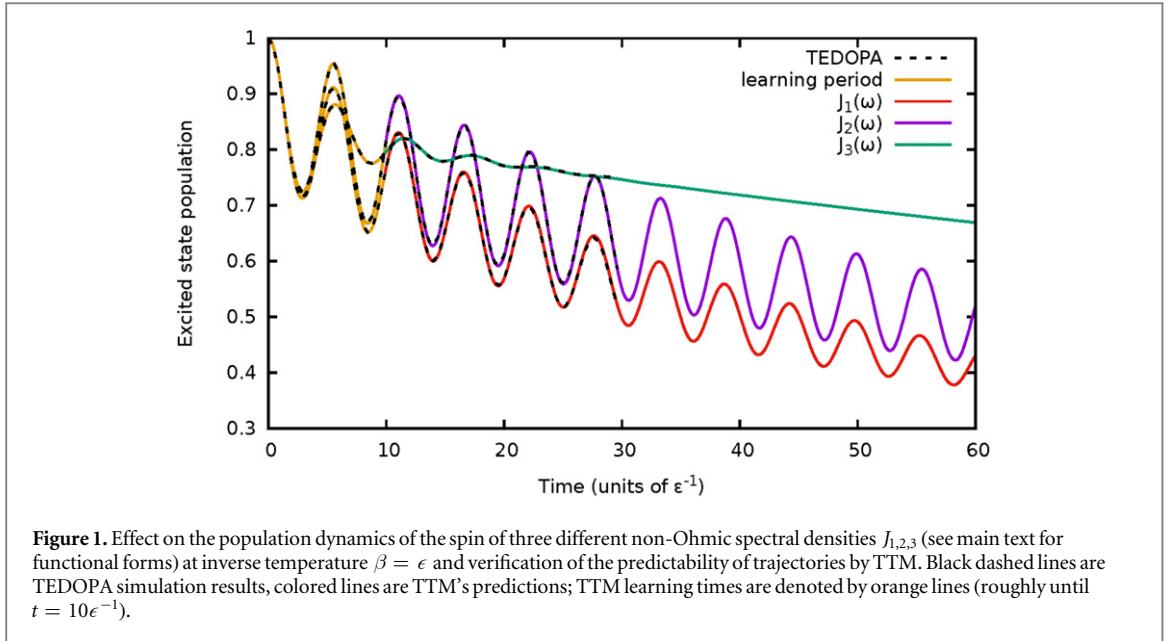
Figure 1. Effect on the population dynamics of the spin of three different non-Ohmic spectral densities $J_{1,2,3}$ (see main text for functional forms) at inverse temperature $\beta = \epsilon$ and verification of the predictability of trajectories by TTM. Black dashed lines are TEDOPA simulation results, colored lines are TTM's predictions; TTM learning times are denoted by orange lines (roughly until $t = 10\epsilon^{-1}$).

Here we set $\hbar = 1$, a convention we will stick to from now on, and express all frequencies in units of ϵ. We employ the standard SBM notation where ϵ corresponds to the energy bias between ground and excited state, Δ is the tunneling matrix element, and σ_i ($i = x, y, z$) are the Pauli matrices corresponding to the i'th spatial direction. The system interaction operator A is defined as the excited state projector $|e\rangle \langle e|$. We choose the parameter $\Delta = 0.6\epsilon$, and an Ohmic spectral density of the Drude–Lorentz form

$$J(\omega) = \lambda\gamma\frac{\omega}{(\omega^2 + \gamma^2)}, \tag{17}$$

with parameters $\lambda = \epsilon$ and $\gamma = 10\epsilon$ respectively identifying a scaling of the interaction strength and a soft cutoff frequency. Thus the bath reorganization energy $\lambda_r = \int J(\omega)\,d\omega$ is $\lambda_r = 5.89\epsilon$. A large hard cutoff $\omega_{hc} = 320\epsilon$ has been employed to meet the aforementioned convergence requirements of TEDOPA under Drude–Lorentz baths.

At an inverse temperature of $\beta = 0.5\epsilon$, TEDOPA exhibits favorable cutoffs and HEOM simulations are accurate, which enables benchmarking. The resulting elements of the memory kernel obtained by TTM applied to TEDOPA's initial trajectories are compared with those retrieved from HEOM [17] simulations of the same system. We have confirmed agreement in a broad range of additional regimes accessible to both TEDOPA and HEOM. Further the system's Hamiltonian has successfully been recovered from the first transfer tensor. This also corroborates the ability of TTM to extract the same dynamical tensors irrespective of the simulation method used for the generation of the trajectories. We will now turn to applications on hitherto inaccessible regimes to illustrate the strengths of the TEDOPA-TTM combination.
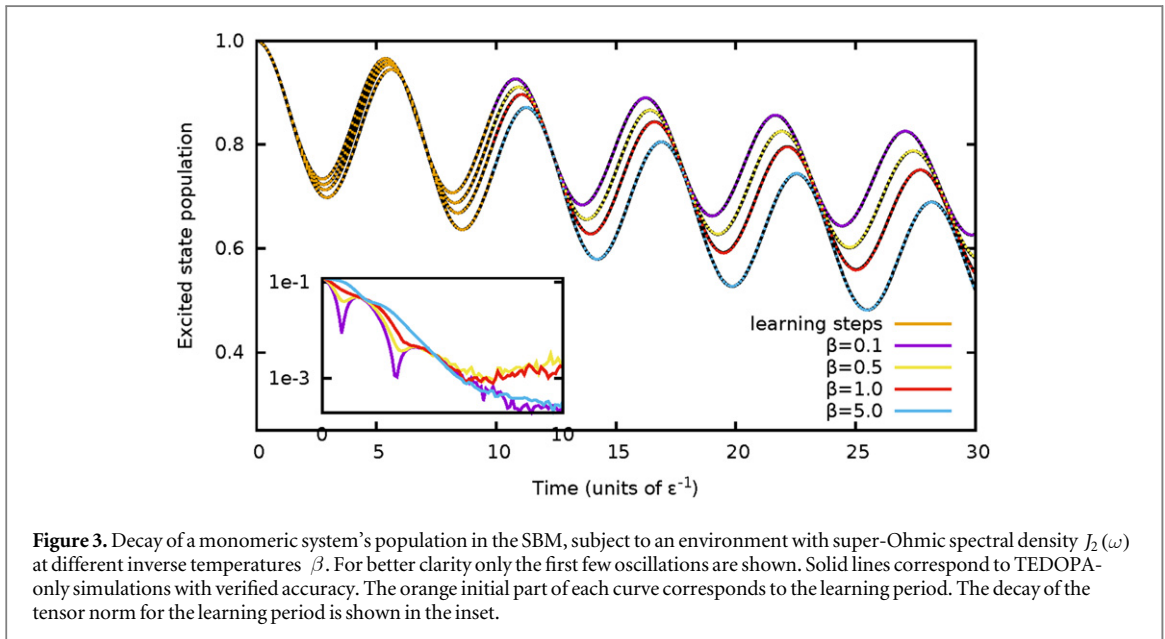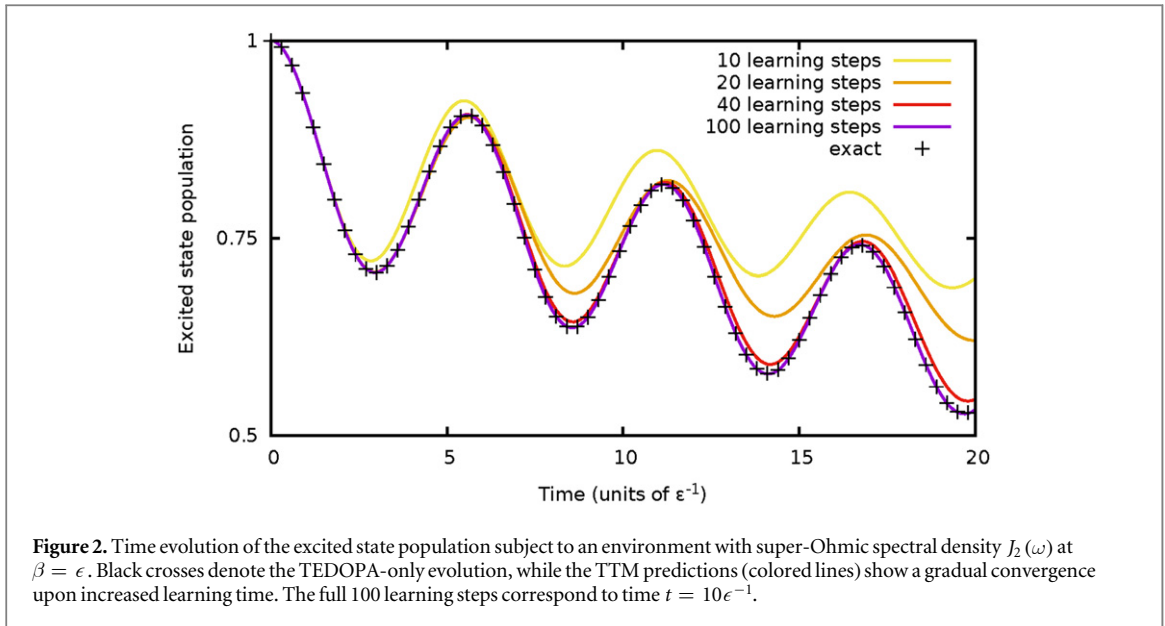
4. Applications

4.1. Non-Ohmic spectra
By construction, TEDOPA is inherently suited to treat spectral densities of arbitrary shape. When considering non-Ohmic spectral densities, Markovian approaches are well-known to anomalously suppress the effect of pure dephasing contributions [58, 59]. In this section we present an analysis of the dynamical effects of three different non-Ohmic spectral densities, namely

$$J_1(\omega) = \lambda_1 \,\omega^3 \,e^{-\omega/\omega_c}, \tag{18}$$

$$J_2(\omega) = \lambda_2 \,\omega^5 \,e^{-\omega/\omega_c}, \tag{19}$$

$$J_3(\omega) = \lambda_3 \,\sqrt{\omega} \,e^{-\omega/\omega_c}. \tag{20}$$

To facilitate comparison, all of them exhibit the same exponential decay with $\omega_c = 0.3\epsilon$ and are subject to a hard cutoff at $\omega_{hc} = 10\epsilon$. Also the parameters $\lambda_1 = 1.8\epsilon$, $\lambda_2 = 1.0\epsilon$ and $\lambda_3 = 0.6\epsilon$ have been chosen in such a way that they all share the same reorganization energy $\lambda_r = 0.3\epsilon$. Thus the average interaction strength between system and environment is the same and the functional form of the spectral density is the factor responsible for disparate dynamics. The resulting dissimilar amplitudes and decay rates of the oscillations due to the different spectral densities are illustrated in figure 1. The tunneling strength is, as in previous section,
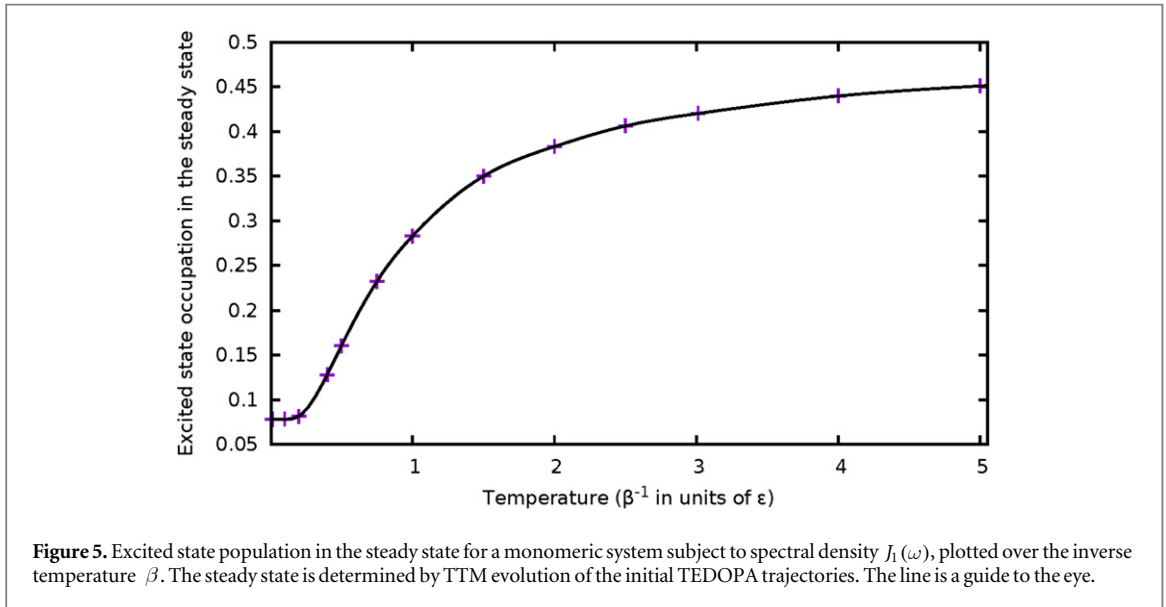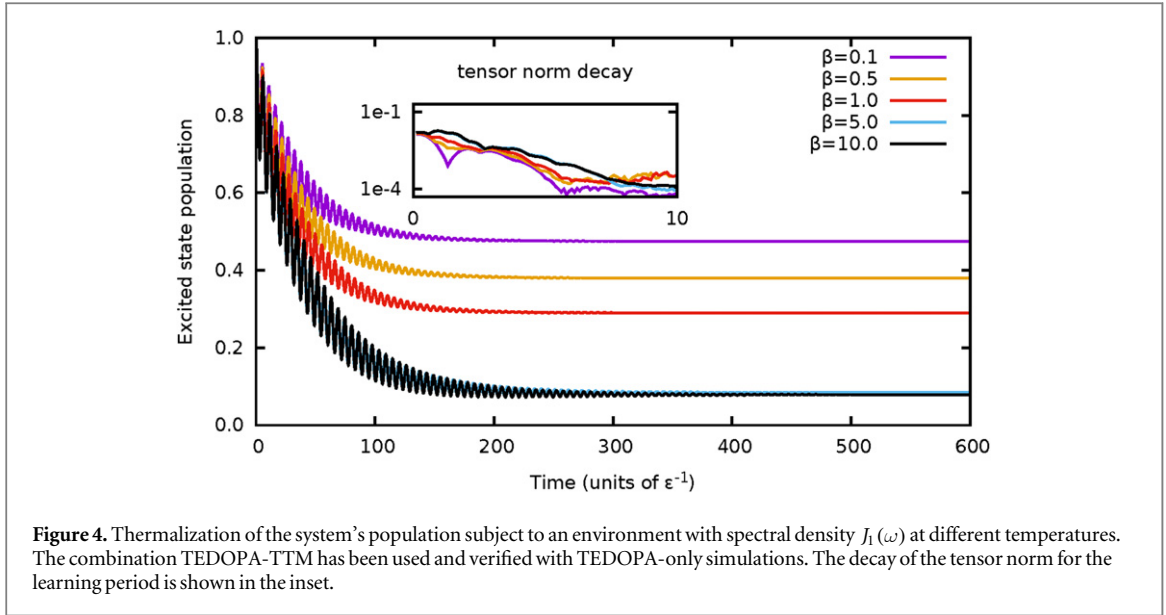
Figure 2. Time evolution of the excited state population subject to an environment with super-Ohmic spectral density $J_2(\omega)$ at $\beta = \epsilon$. Black crosses denote the TEDOPA-only evolution, while the TTM predictions (colored lines) show a gradual convergence upon increased learning time. The full 100 learning steps correspond to time $t = 10\epsilon^{-1}$.

Figure 3. Decay of a monomeric system's population in the SBM, subject to an environment with super-Ohmic spectral density $J_2(\omega)$ at different inverse temperatures β. For better clarity only the first few oscillations are shown. Solid lines correspond to TEDOPA-only simulations with verified accuracy. The orange initial part of each curve corresponds to the learning period. The decay of the tensor norm for the learning period is shown in the inset.

$\Delta = 0.6\epsilon$. One can observe that, for the fastest bath J_2, oscillations are sustained for a longer time, while this ability decreases for spectral densities centered in lower frequencies J_1 and almost disappears for the very slow bath represented by J_3. Some brief initial time is sufficient to generate the transfer tensors and predict the further evolution, whereupon high-accuracy TEDOPA simulations are used to verify these predictions.

The suitability of the TEDOPA-TTM combination is supported by the fact that these simulations require on the order of just 100 tensors to converge to the exact results that have been obtained by full TEDOPA simulations, as shown in figure 2. This translates into about an order of magnitude faster results for TTM-TEDOPA combination than for TEDOPA alone. Further improvements in simulation speed are possible and are discussed in section 4.4.

4.2. Low temperatures
To further illustrate the power of our approach, we present results for a broad range of low to very low temperatures, up to $\beta = 10\epsilon$. For the super-Ohmic spectral density $J_2(\omega)$ we show in figure 3 that it is possible to simulate the dynamics of a monomeric system at various inverse temperatures and the same system parameters as in the previous example. For the case of spectral density $J_1(\omega)$ we employ TTM to propagate the system until the steady state is reached (figure 4) and plot the steady-state occupation of the excited state for

Figure 4. Thermalization of the system's population subject to an environment with spectral density $J_1(\omega)$ at different temperatures. The combination TEDOPA-TTM has been used and verified with TEDOPA-only simulations. The decay of the tensor norm for the learning period is shown in the inset.

Figure 5. Excited state population in the steady state for a monomeric system subject to spectral density $J_1(\omega)$, plotted over the inverse temperature β. The steady state is determined by TTM evolution of the initial TEDOPA trajectories. The line is a guide to the eye.

various inverse temperatures β in figure 5. The insets in figures 3 and 4 show the memory kernel's decay over several orders of magnitude for the corresponding spectral densities. It is this decay which certifies the possibility to use the tensors for long-time propagation of the dynamics.

4.3. Absorption spectrum

The combination of TEDOPA and TTM is especially indicated for applications where accurate simulation of long time dynamics is crucial. The determination of absorption spectra belongs to this class of problems and we analyze here the more complex case of a dimeric system consisting of two coupled monomers.
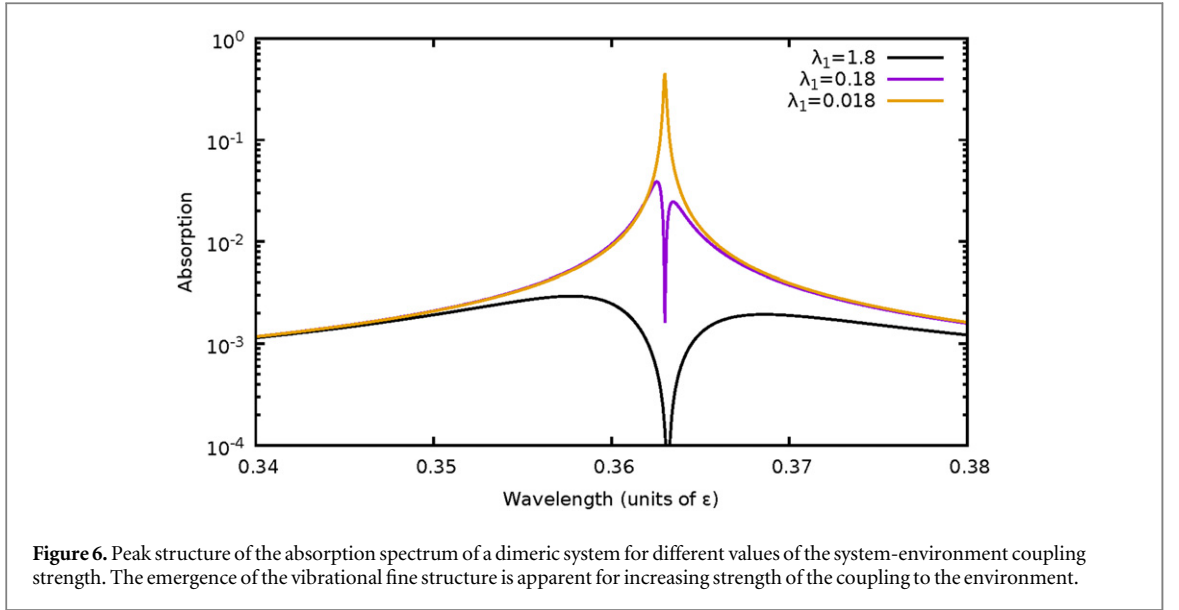
The coupled dimeric system in the single excitation manifold consists of two excited states $|e_1\rangle$, $|e_2\rangle$ and a common ground state $|g\rangle$, and is described by the Hamiltonian

$$H_{\text{sys}} = \epsilon_1|e_1\rangle\langle e_1| + \epsilon_2|e_2\rangle\langle e_2| + J(|e_1\rangle\langle e_2| + |e_2\rangle\langle e_1|), \tag{21}$$

where parameters $\epsilon_1 \equiv \epsilon$, $\epsilon_2 = 2\epsilon$, and exchange interaction strength $J = 0.6\epsilon$ are chosen. Each of the two systems is coupled to a bath. Without loss of generality we assume both environments are described by the same spectral density $J_1(\omega)$ and at temperature $\beta = \epsilon$.

The absorption spectrum is calculated as the Fourier transform of the two point correlation function of the dipole operator $\hat{\mu} = \mu_1|e_1\rangle\langle g| + \mu_2|e_2\rangle\langle g| + \text{h.c.}$

$$C_{\mu-\mu}(t, 0) = \langle \hat{\mu}(t)\hat{\mu}(0)\rangle \tag{22}$$

Figure 6. Peak structure of the absorption spectrum of a dimeric system for different values of the system-environment coupling strength. The emergence of the vibrational fine structure is apparent for increasing strength of the coupling to the environment.

$$= \mathrm{tr}[e^{-iHt}\hat{\mu}e^{iHt}\hat{\mu}\rho(0)], \tag{23}$$

between times $t = 0$ and $t = \tau$ such that the steady state has been reached at τ.

In the limit of weak interaction with the environment, the absorption spectrum emerging from Hamiltonian equation (21) exhibits two peaks in the one-exciton subspace. One of them is shown in the $\lambda_1 = 0.018\epsilon$ line (green) of figure 6, corresponding to the second excited state in the excitonic manifold at a wavelength of around $0.363\frac{c}{\epsilon}$. For higher coupling strengths with the environment, the emergence of the vibrational fine structure splits the peak in two, which is shown in the $\lambda_1 = 0.18\epsilon$ line (blue) and the $\lambda_1 = 1.8\epsilon$ line (black).

It will be interesting to compare the efficiency of the approach presented here with other approaches such as stochastic path integral methods which has recently been developed to calculate absorption and emission spectra [17] specifically for low temperatures and long times.

4.4. Simulation time

The ability of the TEDOPA-TTM combination to explore new simulation regimes is a consequence of the extraordinary savings in computational resources. We will explore these in terms of the 'wall time' t_w, the physical time required for the simulation to be executed as measured by an external clock.

Three factors have a direct influence on simulation time:

- bath coherence time t_{bath},
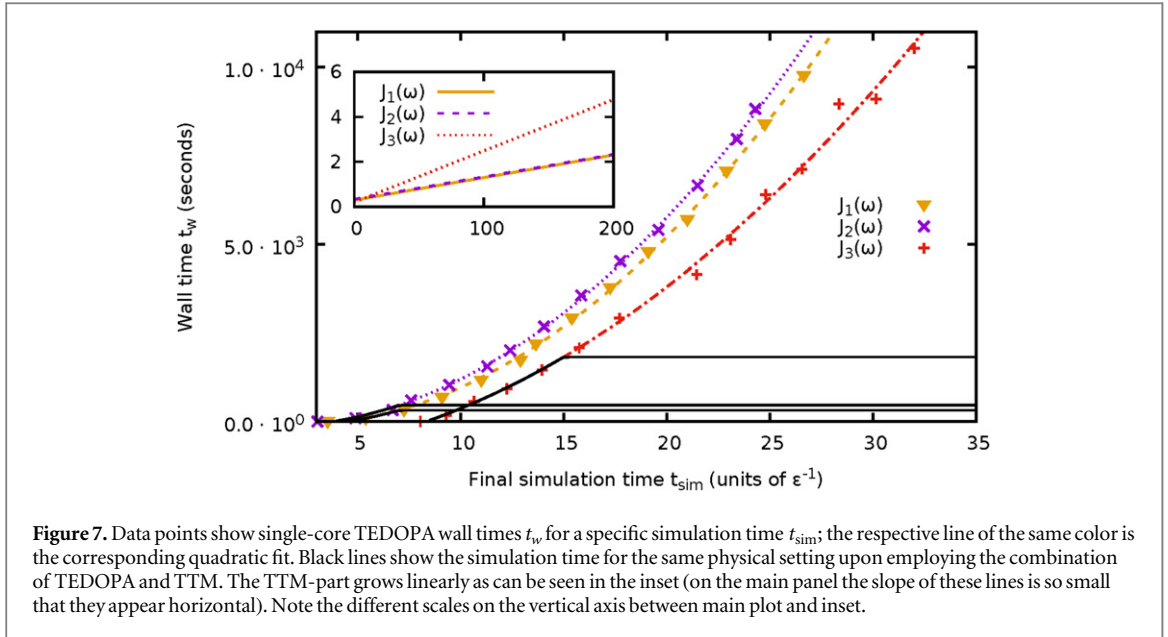
- chain length N and

- system dimension d_{sys}.
  TTM requires the simulation of d_{sys}^2 trajectories until t_{bath}, one for each independent initial density matrix. Although this overhead may become inconvenient for systems of large dimension, the computation may be parallelized to avoid a scaling of t_w with d_{sys}. Even without parallelization, numerical studies often require exploration of a large number of independent initial conditions anyway.

Due to the efficiency of multiplicative propagation with TTM (equation (14)), nearly the totality of the wall time t_w required for a simulation until t_{sim} is employed in the initial generation of the tensors until t_{bath} with TEDOPA. Therefore, one may consider t_w to be essentially independent of t_{sim}. This makes the TTM-TEDOPA combination suitable for long time simulations, i.e. cases where $t_{\mathrm{sim}} \gg t_{\mathrm{bath}}$. There is an additional benefit in shortening simulations with TEDOPA to t_{bath}, since this reduces the necessary chain length N.

The scaling of the wall time t_w necessary to perform a TEDOPA simulation of timestep δt until t_{bath} can be expressed as

$$t_w \propto N \frac{t_{\mathrm{bath}}}{\delta t}\bar{t}, \tag{24}$$

where dependence on three factors has been made explicit: the number of sites N, the number of time steps $\frac{t_{\mathrm{bath}}}{\delta t}$ and a factor $\bar{t}$ denoting the average wall time necessary to simulate one chain site during one time step δt.

Figure 7. Data points show single-core TEDOPA wall times t_w for a specific simulation time t_{sim}; the respective line of the same color is the corresponding quadratic fit. Black lines show the simulation time for the same physical setting upon employing the combination of TEDOPA and TTM. The TTM-part grows linearly as can be seen in the inset (on the main panel the slope of these lines is so small that they appear horizontal). Note the different scales on the vertical axis between main plot and inset.

However, in order to avoid end-of-chain recurrences, for a simulation time t_{bath} one requires

$$N \propto t_{bath} \cdot \bar{v}, \tag{25}$$

sites N in the environment, given an average propagation speed $\bar{v}$ in the chain. Thus a total wall time of

$$t_w \propto \frac{\bar{v}\bar{t}}{\delta t} t_{bath}^2 \equiv c \cdot t_{bath}^2, \tag{26}$$

is needed where c is a scenario-dependent constant.

The global speedup provided by the TTM-TEDOPA combination is illustrated in figure 7 for three instances with different spectral densities. The near independence of t_w on t_{sim} is shown for large t_{sim}. As shown in the inset, in reality t_w increases linearly with t_{sim}, although with a negligible slope. For simulations with TEDOPA alone, the quadratic dependence expressed in equation (26) extends beyond t_{bath} until t_{sim}.

5. Conclusion and outlook

In this work we demonstrated that the combination of TEDOPA and TTM result in an enhanced simulation method of general non-Markovian open-quantum-systems especially well-suited for (but not restricted to) low-temperature regimes and highly structured spectral densities. The formulation in terms of a multiplicative operator whose size is independent of the goal simulation time facilitates exploration of much longer, so far inaccessible timescales.

We verified the feasibility of this combination by a benchmark and presented applications for various spectral densities to highlight the flexibility of our method. Further to the paradigmatic examples presented, even larger benefits can be expected upon application to simulations which are post-processed by some averaging-type method. These are often noise-tolerant or noise-stable, so small deviations do not change the characteristic features of the final result. This type of analysis are expected to be of crucial importance for providing accurate microscopic models of the dynamical behavior of mesoscopic systems and therefore a better understanding of how coherent effects still manifest in those time and length scales [60–63].

Acknowledgments

References

[1] Tahara H, Ogawa Y, Minami F, Akahane K and Sasaki M 2014 *Phys. Rev. Lett.* **112** 147404

[2] Putz S, Krimer D O, Amsüss D, Valookaran A, Nöbauer T, Schmiedmayer J, Rotter S and Majer J 2014 *Nat. Phys.* **10** 720–4

[3] Cai J M, Retzker A, Jelezko F and Plenio M B 2013 *Nat. Phys.* **9** 168

[4] Engel G, Calhoun T, Read E, Ahn T, Mancal T, Cheng Y, Blankenship R and Fleming G 2007 *Nature* **446** 782

[5] Panitchayangkoon G, Hayes D, Fransted K A, Caram J R, Harel E, Wen J, Blankenship R E and Engel G S 2010 *Proc. Natl Acad. Sci. USA* **107** 12766

[6] Collini E, Wong C Y, Wilk K E, Curmi P M G and Scholes G D 2010 *Nature* **463** 644

[7] Breuer H P and Petruccione F 2007 *The Theory of Open Quantum Systems* (Oxford: Oxford University Press)

[8] Rivas Á and Huelga S F 2011 *Open Quantum Systems: An Introduction* (*SpringerBriefs in Physics*) (Berlin: Springer)

[9] Lindblad G 1975 *Commun. Math. Phys.* **40** 147

[10] Gorini V, Kossakowski A and Sudarshan E C G 1976 *J. Math. Phys.* **17** 821

[11] Redfield A 1957 *IBM J. Res. Dev.* **1** 19

[12] Nakajima S 1958 *Prog. Theor. Phys.* **20** 948

[13] Smirne A and Vacchini B 2010 *Phys. Rev. A* **82** 022110

[14] Feynman R P 1948 *Rev. Mod. Phys.* **20** 367

[15] Feynman R P and Vernon F L 1963 *Ann. Phys.* **24** 118

[16] Cao J 1997 *J. Chem. Phys.* **107** 3204

[17] Tanimura Y and Kubo R 1989 *J. Phys. Soc. Japan* **58** 1199

[18] Makri N and Makarov D E 1995 *J. Chem. Phys.* **102** 4611

[19] Leggett A J, Chakravarty S, Dorsey A T, Fisher M P A, Garg A and Zwerger W 1987 *Rev. Mod. Phys.* **59** 1

[20] Diosi L, Strunz W T and Gisin N 1998 *Phys. Rev. A* **58** 1699

[21] Tang Z, Ouyang X, Gong Z, Wang H and Wu J 2015 *J. Chem. Phys.* **143** 224112

[22] Weiss S, Eckel J, Thorwart M and Egger R 2008 *Phys. Rev. B* **77** 195316

[23] Manthe U 2008 *J. Chem. Phys.* **128** 164116

[24] Shi Q and Geva E 2003 *J. Chem. Phys.* **119** 12063

[25] Cohen G and Rabani E 2011 *Phys. Rev. B* **84** 075150

[26] Kidon L, Wilner E Y and Rabani E 2015 *J. Chem. Phys.* **143** 234110

[27] Kapral R 2015 *J. Phys. Condens. Matter* **27** 073201

[28] Kelly A and Markland T E 2013 *J. Chem. Phys.* **139** 014104

[29] Gottwald F, Karsten S, Ivanov S D and Kühn O 2015 *J. Chem. Phys.* **142** 244110

[30] Cao J, Ungar L W and Voth G A 1996 *J. Chem. Phys.* **104** 4189

[31] Egger R, Mühlbacher L and Mak C H 2000 *Phys. Rev. E* **61** 5961

[32] Stockburger J and Grabert H 2002 *Phys. Rev. Lett.* **88** 170407

[33] Mühlbacher L and Rabani E 2008 *Phys. Rev. Lett.* **100** 176403

[34] Moix J M and Cao J 2013 *J. Chem. Phys.* **139** 134106

[35] Baer R and Kosloff R 1997 *J. Chem. Phys.* **106** 8862

[36] Gualdi G and Koch C P 2013 *Phys. Rev. A* **88** 022122

[37] de Vega I 2014 *Phys. Rev. A* **90** 043806

[38] Prior J, Chin A W, Huelga S F and Plenio M B 2010 *Phys. Rev. Lett.* **105** 050404

[39] Chin A W, Rivas A, Huelga S F and Plenio M B 2010 *J. Math. Phys.* **51** 092109

[40] Schollwöck U 2005 *Rev. Mod. Phys.* **77** 259

[41] Cerrillo J and Cao J 2014 *Phys. Rev. Lett.* **112** 110401

[42] Mehraeen S, Cerrillo J and Cao J 2015 in preparation

[43] Cohen G, Gull E, Reichman D R, Millis A J and Rabani E 2013 *Phys. Rev. B* **87** 195108

[44] Wilner E Y, Wang H, Cohen G, Thoss M and Rabani E 2013 *Phys. Rev. B* **88** 045137

[45] Wilner E Y, Wang H, Thoss M and Rabani E 2014 *Phys. Rev. B* **89** 205129
Wilner E Y, Wang H, Thoss M and Rabani E 2014 *Phys. Rev. B* **90** 115145
Wilner E Y, Wang H, Thoss M and Rabani E 2015 *Phys. Rev. B* **92** 195143

[46] Woods M P, Cramer M and Plenio M B 2015 *Phys. Rev. Lett.* **115** 130401

[47] Burkey R and Cantrell C 1984 *J. Opt. Soc. Am. B* **1** 169

[48] Gautschi W 1994 *J. Trans. Math. Softw.* **20** 21

[49] de Vega I, Schollwöck U and Wolf F A 2015 *Phys. Rev. B* **92** 155126

[50] Schollwöck U 2011 *Ann. Phys.* **326** 96

[51] Vidal G 2004 *Phys. Rev. Lett.* **93** 040502

[52] White S R and Feiguin A E 2004 *Phys. Rev. Lett.* **93** 76401

[53] Wolf F A, McCulloch I P and Schollwöck U 2014 *Phys. Rev. B* **90** 235131

[54] Woods M P, Groux R, Chin A W, Huelga S F and Plenio M B 2014 *J. Math. Phys.* **55** 032101

[55] Chin A W, Prior J, Rosenbach R, Caycedo-Soler F, Huelga S F and Plenio M B 2013 *Nat. Phys.* **9** 113

[56] Dijkstra A G, Wang C, Cao J and Fleming G R 2015 *J. Phys. Chem. Lett.* **6** 627

[57] Adolphs J and Renger T 2006 *Biophys. J.* **91** 2778

[58] Wilhelm F W 2008 *New J. Phys.* **10** 115011

[59] Chin A W, Huelga S F and Plenio M B 2012 *Phys. Rev. Lett.* **109** 233601

[60] Huelga S F and Plenio M B 2013 *Contemp. Phys.* **54** 181

[61] Levi F, Mostarda S, Rao F and Mintert F 2015 *Rep. Prog. Phys.* **78** 082001

[62] Scholes G D, Fleming G R, Olaya-Castro A and van Grondelle R 2011 *Nat. Chem.* **3** 763

[63] Mohseni M, Omar Y, Engel G S and Plenio M B (ed) 2014 *Quantum Effects in Biology* (Cambridge: Cambridge University Press)